BIOCHEMISTRY
including biophysical chemistry & molecular biology
Rapid Report

Biochemistry **2009,** *48,* 3807–3809 3807
DOI:10.1021/bi900256q

Conformational Distribution and Ultrafast Base Dynamics of Leadzyme†

Beena M. Kadakkuzha, Liang Zhao, and Tianbing Xia*

Department of Molecular and Cell Biology, The University of Texas at Dallas, Richardson, Texas 75083-0688

Received February 16, 2009; Revised Manuscript Received March 16, 2009

ABSTRACT: The dynamic nature of ribozymes represents a significant challenge in elucidating their structure−dynamics−function relationship. Here, using femtosecond time-resolved spectroscopy and other biophysical tools, we demonstrate that the active site of leadzyme does not have a unique structure, but rather samples an ensemble of conformations that undergo picosecond structural changes. Various base modifications have a profound context-dependent impact on the catalysis.

Leadzyme, a small lead-dependent self-cleaving RNA motif identified by in vitro selection (*1*), features a cleavage site located within an asymmetric purine-rich internal loop (Figure 1A). The cleavage is highly specific for Pb^{2+} ion and is pH dependent (*2*−*4*). The cleavage reaction is unique among known ribozymes in that it undergoes a two-step mechanism (Figure 1A) in which the intermediate 2′,3′-cyclic phosphate product from the first step is specifically hydrolyzed to generate the 3′-mono phosphate product (*5*). Leadzyme's small size makes it an excellent model system for studying the structural and thermodynamic basis of RNA catalysis using NMR (*6*, *7*), crystallography (*8*, *9*), molecular modeling (*10*, *11*), and biochemical and atomic mutational approaches (*2*, *10*, *12*, *13*). These studies produced multiple models that are distinct in subtle but important ways in the precise conformations of the active loop. This suggests that the leadzyme is structurally dynamic (*6*, *14*−*16*), and all the observed structures likely represent a few frames from an ensemble that can be adopted by the motif at ground state in the absence of Pb^{2+} (*9*). The catalytically active form that can be promoted by specific Pb^{2+} binding is not likely present in significant population, and a certain degree of conformational rearrangement is necessary for the in-line nucleophilic attack. Conformational constraints play a significant role (*12*, *13*), so that locking either the bases or sugars in a particular conformation may enhance or reduce catalysis.

We are interested in elucidating the dynamic nature of the active site of leadzyme to understand the role of conformational distribution and dynamic motion on the catalytic activity. We have recently developed an ultrafast spectroscopic approach that allows us to analyze the heterogeneous base stacking patterns for an RNA motif (*17*−*19*). We have designed a series of leadzyme constructs (Table S1, Supporting Information) where 2-aminopurine (P) replaces one of the purine bases in the active site, allowing us to follow the ultrafast quenching dynamics on a picosecond−nanosecond time scale to define the multitude of its stacking interactions with surrounding bases (*19*). Some constructs also carry a second modified base, either 7-deazaguanine (Z) or 7-deazaadenine (X) (Scheme S1, Supporting Information), that quench the fluorescence of P faster than the natural bases of guanine and adenine (*20*), to facilitate assigning site-specific interactions (*17*, *18*). Some also have 8-bromoguanine (8BrG, Scheme S1, Supporting Information) replacing G24. All of these constructs showed similar thermodynamic stabilities (Table S2 and Figure S1, Supporting Information) and circular dichroism profiles (Figure S2, Supporting Information) compared with the WT leadzyme (*21*, *22*).

Catalytic activity, however, is a much more stringent test of the relevance of these constructs. We have developed a high resolution ion-exchange HPLC-based assay for monitoring the kinetic progress of leadzyme self-cleavage, where the uncleaved 30-mer and the cleavage products can be readily resolved (Figure 1B). The WT construct cleaves with an overall kinetic rate constant of $1.4 \pm 0.2\ min^{-1}$ (200 μM Pb^{2+}), independently fitted to the reactant 30-mer and the 6-mer and 24-mer products (Figure 1C), similar to earlier reports for similar conditions (*12*, *13*). In particular, we were able to resolve the two different 6-mer products from the two cleavage steps,that is, the 2′,3′-cyclic phosphate product from the first step and the 3′-mono phosphate product from the second step, in the early time traces, and monitor the conversion from the former to the latter (*5*). Note the individual kinetic rates of initial build up ($2 \pm 0.2\ min^{-1}$) and the subsequent decay of the 2′,3′-cyclic phosphate product that is coupled to the lagging appearance of the 3′-mono phosphate product ($1.3 \pm 0.2\ min^{-1}$). This conversion can be inhibited by the addition of EDTA, suggesting that the second step of the reaction requires the presence of Pb^{2+} ion as well as the structural context of the initial cleavage reaction products of the 6-mer and 24-mer still properly hybridized (*5*, *11*). The total kinetics of combined 6-mers are in agreement with the buildup of 24-mer and the decay of the 30-mer (Figure 1C). It is not clear, however, whether the same or a different bound Pb^{2+} ion is involved in the two separate steps (*3*, *4*, *8*, *10*, *21*, *22*).

The designed constructs showed a range of cleavage activity (Table S3 and Figure S3, Supporting Information), demonstrating various degrees of the influence of the functional group mutations that are highly context dependent. In particular, the P25 construct, where A25 is replaced by P, cleaves 3-fold ($4 \pm 0.1\ min^{-1}$) faster than the WT. It has been suggested that the base at 25 is not directly involved in catalysis, as long as it is not

†This work was supported by the THECB Norman Hackerman Advance Research Program (009741-0004-2006 and 009741-0015-2007) and the Robert A. Welch Foundation (AT-1645).

*To whom correspondence should be addressed. Phone: (972) 883-6328. Fax: (972) 883-2409. E-mail: tianbing.xia@utdallas.edu.

Published on Web 3/23/2009

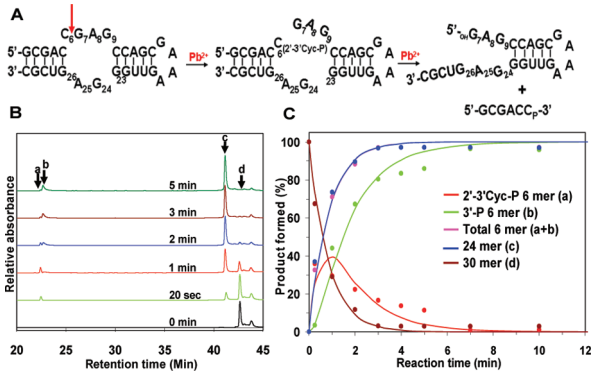

FIGURE 1: Leadzyme motif and cleavage reaction. (A) Secondary structure of leadzyme and two-step cleavage scheme. (B) HPLC time course of WT cleavage reaction. Peaks corresponding to the two 6-mers (a, b), 24-mer (c), and 30-mer (d) are labeled. (C) Fitting of cleavage kinetics for 6-mers, 24-mer, and 30-mer.

a G (presumably not to form a detrimental Watson−Crick base pair with C6), and even an abasic site is as active as the WT (*10*). A faster rate for P25 indicates that the precise location of the exocyclic amino group can influence the transition state energy barrier of the cleavage reaction by either enforcing a favorable local conformation (see below) or by causing conformational changes elsewhere in the loop, or both.

We sought to characterize the conformational ensemble of leadzyme, in particular, the stacking patterns within the internal loop that is relevant to the catalytic mechanism. Figure 2A shows the fluorescence decay dynamics of P25 at pH 6.8, fitted with four unique decay terms (5.2 ps, 33%; 27 ps, 22%; 189 ps, 8%; 11.3 ns, 37%). The multiphasic decay profile suggests a heterogeneous stacking pattern involving this base. The decay profile is very similar to that reported earlier (*18*) of a 5′-dangling end purine base on a GC pair. The base of P has a partial population (55%) that is stacked with G26 and/or G24, reflected in the first two decay components (*18*), but also a significant population that is completely unstacked from the loop (the long nanosecond component, 37%). The unstacked component does not represent a totally unfolded state as such unfolded population is less than 0.05% based on the thermodynamic stability. The assignment of stacking interactions of P25 was facilitated by a comparison with the decay profiles for P25Z26 and P25Z24 (*17*, *18*), where changing G to Z led to faster decays (Table S4, Supporting Information). These findings suggest that there is an equilibrium distribution between partially stacked and unstacked populations at position 25 of the active site.

We also used femtosecond time-resolved anisotropy decay (*18*) to capture the ultrafast base motion of P25 (Figure 2B). Besides a ~10 ns component that represents the tumbling of the entire molecule, there are a 13 ps and a 160 ps component that represent the internal motion of this base (Table S5, Supporting Information). This is again characteristic of a 5′-dangling purine base (*18*). As demonstrated before, the 13 ps component corresponds to local base motion about the glycosidic bond, and the 160 ps component corresponds to base stacking and unstacking motions. These motions allow the base to sample various stacked and unstacked states and their detection confirms the flexible nature of the active loop (*6*, *16*). These motions also act to gate the charge transfer between P and surrounding quencher bases, leading to the apparent quenching rates on such similar time scales. In other words, the first decay component (5.2 ps) is due to quenching by a statically stacked G26, and the second (27 ps) and

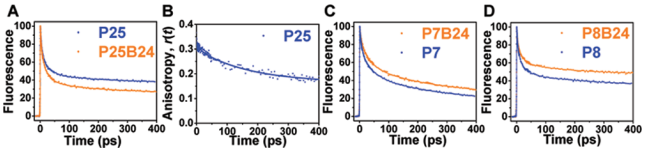

FIGURE 2: Ultrafast dynamic decay profiles of leadzyme constructs. (A) P25 and P25B24. (B) Anisotropy decay of P25. (C) P7 and P7B24. (D) P8 and P8B24.

third (189 ps) components are mostly due to conformational dynamics-gated quenching.

NMR (*7*) and crystallographic studies (*8*, *9*) showed that A25 is stacked intrahelically forming a pair with C6 in the ground state, and NMR relaxation measurements showed that the dynamics of A25 are similar to those of helical regions at pH 5.5, with a population distribution of 10:1 between protonated and unprotonated states (*7*). The MC-Sym model, however, suggests that this base is bulged out for catalysis (*10*, *11*). Unpairing of A25 from C6 is necessary for transition to the active conformation (*6*, *7*, *16*), allowing C6 to form a base triple with G9 and G24 (*10*, *13*). The phenomenon of opening of alternative base pairs for ligand recognition or proper folding has also been observed in other RNA systems, for example, theophylline aptamer (*23*) and purine riboswitch RNAs (*24*−*26*). Although P25 is capable of forming a base pair with C6 at either neutral or low pH (*27*), the pair is not as stable, leading to a lower energetic penalty and enhanced catalysis (*16*). At pH 5.5, the stacking population is slightly enhanced (Figure S5, Supporting Information), similar in trend with results of the NMR studies (*7*). Another possible source of catalytic enhancement may come from the P base adopting a partial *syn* conformation due to the amino group being in the 2-position, analogous to guanine which is known to prefer the *syn* conformation more readily than do other bases. We note that the *syn* conformation favored by 6-methyl U at this position also enhances the cleavage rate (*10*).

Other positions that are modified with P, or together with Z or X, reduce the activity by different degrees (Table S3, Supporting Information). A strong correlation is evident that those modifications that interfere with the formation of the C6−G9−G24 base triple either significantly diminish the activity or render the constructs totally inactive. For example, for P25Z24, where one single hydrogen bond involving the N7 of G24 is disrupted, the activity is completely abolished. These findings further support that this base triple is on the pathway toward the transition state, although it may not be present in significant population at the ground state. Modification of guanine bases at 23 (P25Z23) and 26 (P25Z26) by Z reduce the activity by 6- and 20-fold, respectively, compared with P25, in agreement with earlier observations (*10*). Purine N7 is the best nucleophile of the nucleobases, most likely to be metal binding sites. The observed reduced activity is likely due to interference of Pb^{2+} binding by mutations at the N7 of these guanine bases.

Positions 7 and 8 have not been found to be totally conserved, but purines are preferred (*2*, *10*), and constructs with P, Z, or X at these positions can undergo complete cleavage yet with slower rates (Table S3, Supporting Information). Precise base stacking patterns involving these bases differ in the NMR solution structure, the crystal structures, and the MC-Sym model (*7*−*10*). Figure 2C,D shows the decay dynamics of constructs P7 and P8. Similar to that of P25, these multiexponential decay profiles (Table S4, Supporting Information) indicate multiple subpopulations that each have a different mode of base−base

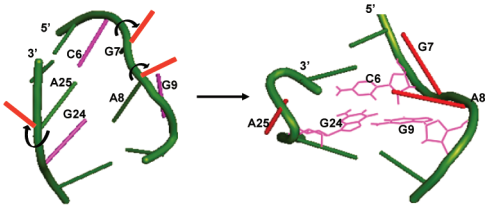

FIGURE 3: Conformational heterogeneity of leadzyme and transition to active state of base triple model. Major (green, based on NMR structure) and minor (red) base stacking patterns for 7, 8, and 25, and the base triple of C6-G9-G24 (pink) are indicated.

interactions. The lack of ~1 ps component from certain constructs, for example, P8Z7 and P8Z9, suggests that adjacent bases on the longer strand are not well stacked within the loop. In the single stranded state, however, ~1 ps components were observed when P8 is adjacent to Z7 or Z9 (Table S4, Supporting Information), indicating that it is the internal loop context that causes the lack of perfect base stacking. NMR studies showed that the A8 sugar dynamically fluctuates between C3′- and C2'-endo conformations on subns time scales (*6*). Femtosecond anisotropy decay showed a main component of 137 ps for the internal motion of this base (Table S5, Supporting Information), complementing the NMR results on the sugar moiety. Although shown to be mostly intrahelical, G24 flips out in about 20% of the NMR structures (*7*). In MC-Sym, G24 partially stacks on G23 (*11*). Although P at 24 renders the relevant constructs, for example, P24 and P24Z23, totally inactive, the decay dynamics for these constructs (Table S4, Supporting Information) indicate that on average in ~70% of the population the base P24 is stacked with G23, similar to that of P as a 3′-dangling end on a GC pair (*18*).

It has been demonstrated recently that separate incorporations of an 8BrG (B) base at the three guanine positions in the active site each resulted in different effects on the activity (*13*). In particular, 8BrG at G24 was shown to enhance the cleavage activity by 3−30 fold. We also observed a 3−25 fold enhancement of activity upon 8BrG-24 substitution (Table S3, Supporting Information), as long as the original construct without 8BrG had at least residual activity. In particular, construct P25B24 had hyperactivity beyond our ability to capture the initial reaction using the HPLC assay, suggesting an additivity of the enhancement effects of P at 25 and 8BrG at 24. For totally inactive constructs (e.g., P9), however, 8BrG-24 could not rescue the activity, consistent with the notion that the integrity of the C6−G9−G24 base triple is crucial. We proceeded to examine whether 8BrG substitution at 24 changed the distribution of conformations elsewhere in the loop such that the transition state energy barrier was lowered. We first confirmed that 8BrG quenches P similar to quenching by the natural base G (Table S4, Supporting Information) using a 5′-GBP-3′ trimer to mimic the local sequence of G23−G24−A25. Figure 2A,C,D shows a comparison of ultrafast decay dynamic profiles with G and with 8BrG at position 24. The 8BrG modification enhances the overall population of stacking interactions for P25. The base A25 is bulged out in the catalytically relevant base triple model. Therefore, the change in stacking at P25 cannot be the main mechanism of enhanced activity. For both P7 and P8, 8BrG-24 moderately increases the overall unstacked populations. This is consistent with the fact that both bases need to flip out to allow the formation of the C6−G9−G24 triple. Therefore, it is likely that 8BrG-24 enhances leadzyme activity partially by enforcing a favorable conformational distribution at these two bases, in addition to favoring a *syn* conformation at G24 (*13*).

In summary, we sought to establish the correlation between conformational heterogeneity and dynamics of leadzyme's active site with its catalytic potential. The active site is very dynamic and is not one unique structure. The intrinsic tendency for purine bases to act as the dangling end (*18*) dominates their dynamic behavior. On the basis of the observed population distribution, the $\Delta G°$ values between different states are within 1 kcal/mol, and the picosecond fast base motion suggests that the energy barrier for interconversion between certain conformations is very low. As demonstrated before (*16*), there is a balance between orderliness and dynamics, and the presence of multiple independent motions and heterogeneity at the active site has a significant impact on ribozyme function (*6*, *13*).

ACKNOWLEDGMENT

We thank Dr. Philip Bevilacqua for stimulating discussions and Dr. Donald Gray for critical reading of the manuscript.

SUPPORTING INFORMATION AVAILABLE

Materials and experimental procedures; tables of constructs, thermodynamic and fluorescence decay parameters; figures of UV melting, CD spectra, ultrafast fluorescence decays. This material is available free of charge via the Internet at http://pubs.acs.org.

REFERENCES

1. Pan, T., and Uhlenbeck, O. C. (1992) *Biochemistry 31*, 3887–3895.
2. Pan, T., Dichtl, B., and Uhlenbeck, O. C. (1994) *Biochemistry 33*, 9561–9565.
3. Sugimoto, N., and Ohmichi, T. (1996) *FEBS Lett. 393*, 97–100.
4. Ohmichi, T., and Sugimoto, N. (1997) *Biochemistry 36*, 3514–3521.
5. Pan, T., and Uhlenbeck, O. C. (1992) *Nature (London) 358*, 560–563.
6. Legault, P., Hoogstraten, C. G., Metlitzky, E., and Pardi, A. (1998) *J. Mol. Biol. 284*, 325–35.
7. Hoogstraten, C. G., Legault, P., and Pardi, A. (1998) *J. Mol. Biol. 284*, 337–350.
8. Wedekind, J. E., and McKay, D. B. (1999) *Nat. Struct. Biol. 6*, 261–268.
9. Wedekind, J. E., and McKay, D. B. (2003) *Biochemistry 42*, 9554–9563.
10. Chartrand, P., Usman, N., and Cedergren, R. (1997) *Biochemistry 36*, 3145–3150.
11. Lemieux, S., Chartrand, P., Cedergren, R., and Major, F. (1998) *RNA 4*, 739–749.
12. Julien, K. R., Sumita, M., Chen, P. H., Laird-Offringa, I. A., and Hoogstraten, C. G. (2008) *RNA 14*, 1632–1643.
13. Yajima, R., Proctor, D. J., Kierzek, R., Kierzek, E., and Bevilacqua, P. C. (2007) *Chem. Biol. 14*, 23–30.
14. Mueller, L., Legault, P., and Pardi, A. (1995) *J. Am. Chem. Soc. 117*, 11043–11048.
15. Legault, P., and Pardi, A. (1997) *J. Am. Chem. Soc. 119*, 6621–6628.
16. Hoogstraten, C. G., Wank, J. R., and Pardi, A. (2000) *Biochemistry 39*, 9951–9958.
17. Zhao, L., and Xia, T. (2007) *J. Am. Chem. Soc. 129*, 4118–4119.
18. Liu, J. D., Zhao, L., and Xia, T. (2008) *Biochemistry 47*, 5962–5975.
19. Xia, T. (2008) *Curr. Opin. Chem. Biol. 12*, 604–611.
20. Wan, C. Z., Xia, T. B., Becker, H. C., and Zewail, A. H. (2005) *Chem. Phys. Lett. 412*, 158–163.
21. Kim, M. H., Katahira, M., Sugiyama, T., and Uesugi, S. (1997) *J. Biochem. 122*, 1062–1067.
22. Katahira, M., Kim, M. H., Sugiyama, T., Nishimura, Y., and Uesugi, S. (1998) *Eur. J. Biochem. 255*, 727–733.
23. Zimmermann, G. R., Shields, T. P., Jenison, R. D., Wick, C. L., and Pardi, A. (1998) *Biochemistry 37*, 9186–9192.
24. Noeske, J., Schwalbe, H., and Wohnert, J. (2007) *Nucleic Acids Res. 35*, 5262–5273.
25. Lemay, J. F., and Lafontaine, D. A. (2007) *RNA 13*, 339–350.
26. Mulhbacher, J., and Lafontaine, D. A. (2007) *Nucleic Acids Res. 35*, 5568–5580.
27. Sowers, L. C., Boulard, Y., and Fazakerley, G. V. (2000) *Biochemistry 39*, 7613–7620.